We are IntechOpen,
the world's leading publisher of
Open Access books
Built by scientists, for scientists

6,900
Open access books available

185,000
International authors and editors

200M
Downloads

154
Countries delivered to

Our authors are among the

TOP 1%
most cited scientists

12.2%
Contributors from top 500 universities

BOOK CITATION INDEX
CLARIVATE ANALYTICS
INDEXED

WEB OF SCIENCE™

Selection of our books indexed in the Book Citation Index
in Web of Science™ Core Collection (BKCI)

Interested in publishing with us?
Contact book.department@intechopen.com

Numbers displayed above are based on latest data collected.
For more information visit www.intechopen.com

Numerical Modeling of Reflector Antennas

Oleg A. Yurtcev and Yuri Y. Bobkov
Belarusian state university of informatics and radioelectronics
Belarus

1. Introduction

The numerical modeling of reflector antennas is a necessary stage of their design. Due to numerical modeling dimensions of all antenna elements are defined. The more factors are accounted during antenna numerical modeling the more accurately the antenna elements dimensions are defined. There are many methods used in the programs of antenna numerical modeling: geometric optics method; aperture method; geometric theory method of diffraction; physical optics method, integral equations method; finite elements method. By now there are many papers in which the different aspects of reflector antenna numerical modeling are discussed. For determination of the field antenna reflector in regions of main lobe and first side lobes in front semi-space the aperture method is used; for determination of the field in full semi-space the physical optics method is used (Chen & Xu, 1990; Charles, 1975; Rusch, 1974). The geometric theory of diffraction (Narasimhan & Govind, 1991; Rahmat-Samii, 1986; Narasimhan et al, 1981) and moment method (Khayatian & Rahmat-Samii, 1999) are used for determination of the field in back semi-space, for determination of field features in front semi-space related with diffraction of the field on the edge of paraboloid and hyperboloid surfaces and for modeling the feed-horn. In a number of papers different approaches are used for simplification of analytical expressions for calculation of antenna fields to reduce a mathematical model of antenna and to simplify modeling program (Rahmat-Samii, 1987). A number of works deal with research into the field in near-field zone (Narasimhan & Christopher, 1984; Fitzgerald, 1972; Houshmand et al., 1988; Watson, 1964). But the results are not reduced to numerical data in that volume which is necessary for antenna design. The field distribution in near-field zone is described in detail for plane aperture at uniform its excitation (Laybros et al., 2005), but for reflector antennas such research was not provided. The reflector antenna in receiving mode is not discussed in literature, however at designing antenna for radioimaging systems it is necessary to know of field distribution in the focal region at receiving of the wave from near-field zone points. The issue of isolation of channels in multi-beam reflector antenna at receiving of the wave from near-field zone is not analyzed too. Without analysis of the isolation between channels it is impossible to analyze the quality of imaging in radioimaging systems.

In literature a number of works deal with describing the feed-horns in monopulse reflector antennas (Hannan, 1961; Scolnic, 1970). There is a little information on numerical characteristics description the regularity in monopulse reflector antenna.

In the present chapter the mathematical model of the single-reflector paraboloid antenna and double-reflector paraboloid Cassegrain antenna is based on physical optics method

with the same features in comparison with frequently used models. These features are the following:

a) the feed-horn in the form of the pyramidal horn is not accurate; a limited feed-horn aperture dimensions, its depth and influence of these dimensions on distribution of the amplitude and phase of the field on the horn aperture are assumed; the feed-horn field is determined based on amplitude and phase of the field on the aperture by Kirchgoff integral;

b) it is supposed that paraboloid in single-reflector and hyperboloid in double-reflector antenna are located on the prefixed distance from feed-horn aperture plane (the approximation of the far-field zone is not used);

c) paraboloid in the double-reflector antenna is located on the unknown distance from hyperboloid (the approximation of the far-field zone is used);

f) in radiation mode, the point, in which the field is defined, is located in any zone of space (far-field, intermediate, near-field); in receiving mode the point of spherical wave source is located also in any space zone.

The geometrical theory of diffraction is used only for analysis of the field in back semi space, but in the chapter the analysis results are not present. Using of Kirchgoff integral for calculation of the field of feed-horn (in radiation mode), waveguide excitation theory (in receiving mode) and physical optics method at determination of the field of hyperboloid and paraboloid allow to avoid limitations on wave dimensions of the paraboloid. Simulation time of problem and needed memory value of computer is less than for universal electromagnetic simulation programs such as CST MICROWAVE STUDIO, HFSS, FEKO. The modeling accuracy is about the same.

2. Mathematical model of reflector antenna in radiation and receiving modes

2.1 Antenna geometry

The single-reflector and double-reflector Casserrain antenna (reflector is parabolic, sub-reflector is hyperbolic) are analyzed in this work. The double-reflector antenna within coordinate system X,Y,Z and its geometric dimensions are shown in figure 1. The antenna elements involved are: 1 – paraboloid; 2 – hyperboloid; 3 – feed horn; 4 – rectangular waveguide. Antenna element dimensions and markings are the following: F_h – phased center of feed horn; F –parabolic focus; D_p – parabolic diameter; D_g – hyperboloid diameter; F_P – parabolic focus distance; F_{g1} – far focus hyperboloid distance; F_{g2} – near focus hyperboloid distance; $2\theta_{M\,max}\ 2\Theta_0$ – parabolic aperture angle; M – point on parabolic surface; $R_M, \theta_M, \varphi_M\ R_M, \theta_M, \varphi_M$ – spherical coordinates of M point with respect to parabolic focus F.

The space point P is shown in fig2. It is in this point that the field is determined in this point in radiation mode. In receiving mode the EM-field source is located in point P. The position of point P is set by spherical coordinates R, θ, φ. The projection of P point on XY-plane is shown in figure 2 as Pxy point with coordinates R, θ, φ.

The combination of physical optics method (PO) and geometric theory of diffraction (GTD) are used in mathematical model of reflector antenna in the radiation mode. The physical optics method is used for calculation of field in front semi-space (θ<90°). The GTD method is used in mathematical model of reflector antenna for calculation field in back semi-space (θ>90°). The point P is located only in front semi-space for receiving mode and antenna is analyzed by physical optics method. The theory of waveguide excitation is used for calculation of power level on waveguide input.

Fig. 1. Double-reflector antenna

2.2 Single-reflector antenna in radiation mode

Pyramidal horn is used as feed-horn. The feed horn is executed by rectangular waveguide – figure 3. The horn dimensions A_h, B_h are aperture dimensions, R_h is horn depth. The case when polarization plane of feed horn coincides with YZ plane is considered. The dimension of waveguide cross section satisfy a uniqueness condition of wave TE_{10} : $a < \lambda < 2a$, where λ – wavelength.

The mathematical model includes the following known equations.

The complex amplitude of field in a rectangular waveguide at horn input:

$$\overset{\bullet}{E}_y = E_m \cos(\pi x / a) \tag{1}$$

where a- is the dimension of the wide wall of rectangular waveguide;

$E_m = \sqrt{Ps \cdot Z / (a \cdot b)}$ - is electric field amplitude in the center of side «a» of the waveguide.

$Z = 120\pi / \sqrt{\varepsilon[1 - (\lambda / 2a)^2]}$ - is characteristic impedance of the waveguide;

ε - is related permittivity of waveguide internal environment.

Further an approximation is used: the wave in feed horn has spherical wave front. The wave source is located in horn vertex – in point O in figure 3. In this wave the field phase Ψ along the direction R_{oq} from horn vortex to Q point on aperture Sh is changed according to the law: $\Psi = 2\pi R_{oq} / \lambda$. The field amplitude is changed proportionally $1 / R_{oq}$. As a result of it the distributions of field phases $\Psi_s(x, y)$ and field amplitudes $E_s(x, y)$ on the horn aperture are calculated by expressions:

Fig. 2. Antenna and point P in space.

Fig. 3. Rectangular waveguide and feed horn

$$\Psi_s(x,y) = -2\pi \cdot [R_{oq}(x,y) - R_{oq}(0,0)]/\lambda \, ;$$
$$E_s(x,y) = E_m R_{oq}(0,0)\cos(\pi x/A_h)/R_{oq}(x,y)$$

(2)

where E_m is amplitude of field in the center of wide waveguide wall;

$$R_{oq}(x.y) = \sqrt{R_h^2 + x^2 + y^2} \, ; \quad -0{,}5A_h \leq x \leq 0{,}5A_h \, ;$$
$$-0{,}5B_h \leq y \leq 0{,}5B_h$$

(3)

The field on paraboloid surface is calculated by Kirchhoff integral according to the field on aperture. The field is calculated in arbitrary point M having rectangular coordinates X_M, Y_M, Z_M and spherical coordinates R_M, θ_M, φ_M (see fig.1).

$$\vec{E}_M \approx i\frac{1}{2\lambda}\int_{S_h} E_s\left[\vec{\theta}_o(\eta\cos\theta_M+1)\cos\varphi_M - \vec{\varphi}_M(\cos\theta_M+\eta)\sin\varphi_M\right]\frac{\exp(i\Psi_s-ikR_{QM})}{R_{QM}}dS \quad (4)$$

where E_s, Ψ_s are determined by equations (2); $\eta = \sqrt{1-(\lambda/2Ah)^2}$; $i = \sqrt{-1}$; k=2π/λ; $\vec{\theta}_o, \vec{\varphi}_o$ are unit vectors of spherical coordinate system R_M, θ_M, φ_M; R_{QM} is the distance from point Q on horn aperture (see fig.3) to point M on the paraboloid surface. This distance is expressed in terms of rectangular coordinates of Q, M points in the coordinate system, with the geginning being in the point of paraboloid vortex O_p (see fig.4). The center of feed-horn aperture feed-horn (point Q_S) is shifted from paraboloid focus point (point F) at coordinates X,Y,Z on values D_{hx}, D_{hy}, D_{hz}. This would provides an antenna focusing in well known point P of any space zone.
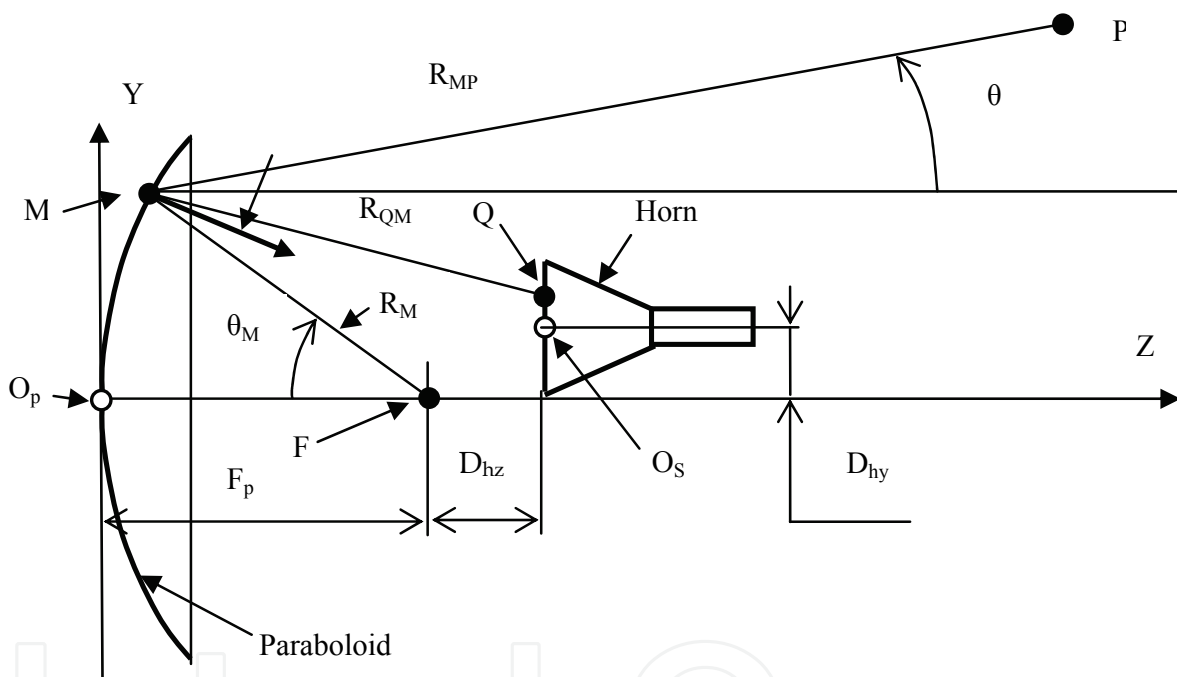
Fig. 4. Single-reflector antenna with feed horn

The expression for R_{QM} results from figure 4 by means of rectangular coordinates of the point Q and M in X,Y,Z coordinate system.

$$R_{QM} = \sqrt{(x_Q-x_M)^2+(y_Q-y_M)^2+(z_Q-z_M)^2},$$
$$x_Q = D_{hx}+x; \quad y_Q = D_{hy}+y; \quad z_Q = D_{hz}+z \quad (5)$$

$$x_M = 2F_p\sin\theta_M\cos\varphi_M/(1+\cos\theta_M); \quad y_M = 2F_p\sin\theta_M\sin\varphi_M/(1+\cos\theta_M);$$
$$z_M = F_p[1-2\cos\theta_M/(1+\cos\theta_M)] \quad (6)$$

The angles θ_M, φ_M are calculated by coordinates x_M, y_M, x_Q, y_Q using relations:

$$\sin\theta_M = \sqrt{(x_M - x_Q)^2 + (y_M - y_Q)^2} / R_{QM};$$
$$\operatorname{tg}\varphi_M = (x_M - x_Q)/(y_M - y_Q) \tag{7}$$

The point M on the paraboloid surface is the point of crossing of two line systems, which are the paraboloid surface lying in XZ and YZ planes. The distance between lines on coordinates X and Y are marked as ΔX and ΔY. The values of ΔX and ΔY are selected according to the criterion of convergence of the calculations of side lobe levels and antenna gain, i.e. by parameters which are most critical to $\Delta X/\lambda$ and $\Delta Y/\lambda$ values. The results of numerical modeling show that the $\Delta X/\lambda > 3$ and $\Delta Y/\lambda > 3$ are sufficient.

The vector of the magnetic field $\vec{H}_M$ in point M and than the vector of surface current density are determined in terms of the field $\vec{E}_M$. In conformity with PO method:

$$\vec{J}_s = 2[\vec{n}_0, \vec{H}_M] = \vec{J}_x + \vec{J}_y + \vec{J}_z \tag{9}$$

where $\vec{J}_x, \vec{J}_y, \vec{J}_z$ are components of $\vec{J}_s$ vector in rectangular coordinate system depending on M point coordinates x_M, y_M, z_M; the $\vec{n}_0$ is a unit vector perpendicular to paraboloid surface in point M.

The vector potential $\vec{A}$ method is used for determination of $\vec{E}$ field of the currents $\vec{J}_x, \vec{J}_y, \vec{J}_z$ in the point P (see figures 2, 4):

$$\vec{E} \approx -i\frac{60\pi}{\lambda}\vec{A} = \vec{E}_x + \vec{E}y + \vec{E}_z; \quad \vec{A} = \int_{S_p} \vec{J}_s \frac{\exp(-ikR_{MP})}{R_{MP}} dS;$$
$$R_{MP} = \sqrt{(x_M - x_P)^2 + (y_M - y_P)^2 + (z_M - z_P)^2} \tag{10}$$

where S_p are paraboloid surfaces.

The rectangular coordinates of P point x_p, y_p, z_p are associated with spherical coordinates R, θ, φ as:

$$x_P = R\sin\theta\cos\varphi; \quad y_P = R\sin\theta\sin\varphi; \quad z_P = R\cos\theta \tag{11}$$

The vector $\vec{E}$ projections on unit vectors $\vec{\theta}_o$ и $\vec{\varphi}_o$ are determined by expressions:

$$E_\theta = (E_x \cos\varphi + E_y \sin\varphi)\cos\theta - E_z \sin\theta;$$
$$E_\varphi = (-E_x \sin\varphi + E_y \cos\varphi)\cos\theta \tag{12}$$

Fig. 5. Spherical coordinates system

The antenna directivity diagrams $F_\theta(\theta,\varphi)$, $F_\varphi(\theta,\varphi)$ and antenna gain G are calculated based on E_θ и E_φ components.

$$G = E_{max}^2 R^2 / 60 P_s \qquad (13)$$

Where E_{max} is the maximum value of the electric field amplitude on sphere R=const; P is radiation power.

2.3 A single-reflector antenna in receiving mode.

A reflector antenna can receive a spherical wave from any points of far, intermediate and near field zones space. Let a spherical wave source be located in the point P shown in fig. 4. The amplitude of the wave electric field of is equal E_i. It is necessary to calculate power P_i entering the waveguide. The algorithm of power P_i calculation includes the following steps:

Step 1. The vector of surface current on paraboloid surface is calculated based on the spherical wave magnetic field $\vec{H_i}$ and the wave propagation direction using the formula similar to (9).

Step 2. The field $\vec{E_s}$ in the point $Q(x_Q, y_Q, z_Q)$ on feed horn aperture is calculated by components $\vec{J_x}, \vec{J_y}, \vec{J_z}$ of surface current $\vec{j_s}$ using the formula similar to (10)

$$\vec{E_S} \approx -i\frac{60\pi}{\lambda}\vec{A} = \vec{E_x} + \vec{E}y + \vec{E_z} \ ;$$

$$\vec{A} = \int_{S_p} \vec{J_s} \frac{\exp(-ikR_{MQ})}{R_{MQ}} dS \ ; \qquad (14)$$

$$R_{MQ} = \sqrt{(x_M - x_Q)^2 + (y_M - y_Q)^2 + (z_M - z_Q)^2}$$

Step 3.   The amplitude of TE_{10} wave in the rectangular waveguide is defined by $\vec{E}_s$ field. This problem is solved by the own wave method using the waveguide excitation theory.

In conformity with this theory the $\vec{E}$ and $\vec{H}$ field in waveguide is presented as the sum of the own waveguide waves $\vec{E}_\nu$ and $\vec{H}_\nu$, where ν is generalized index describing a wave type and its propagation direction:

$$\vec{E} = \sum_{(\nu)} C_\nu \vec{E}_\nu \, , \quad \vec{H} = \sum_{(\nu)} C_\nu \vec{H}_\nu \tag{15}$$

where C_ν is an excitation coefficient related to off-site sources – the density of off-site electric current $\vec{J}_e$ and magnetic $\vec{J}_h$ currents:

$$C_\nu = \frac{1}{N_\nu} \int_V \left[\vec{J}_e \vec{E}_{-\nu} - \vec{J}_h \vec{H}_{-\nu} \right] dV \tag{16}$$

where V is the volume in which the off-site sources of the field are located; N_ν is the norm, given by

$$N_\nu = \int_S \{ [\vec{E}_\nu, \vec{H}_{-\nu}] - [\vec{E}_{-\nu}, \vec{H}_\nu] \} \vec{m}_0 dS \tag{17}$$

In equations (14)-(16) the $\vec{E}_\nu, \vec{H}_\nu$ are advanced own waves; $\vec{E}_{-\nu}, \vec{H}_{-\nu}$ are reversed own waves; S is a waveguide cross-section area; $\vec{m}_0$ is a unit vector perpendicular to the waveguide cross-section.

The equations concerned are used for solution of problems of TE_{10} wave excitation in the rectangular waveguide with cross-section dimensions A_h and B_h without accounting transformation of the waveguide to aperture horn. It is assumed that other waves except TE_{10} cannot propagate. The integration in (15) is carried out on the horn aperture. On the horn aperture the vector $\vec{J}_e$ =0, and vector $\vec{J}_h$ is expressed by the field $\vec{E}_S$ component tangent to horn aperture. The axis of excited waveguide is oriented along the Z-axis. In this case the $\vec{m}_0 = \vec{z}_0$, where $\vec{z}_o$ is a unit vector parallel to the Z-axis. The vector $\vec{J}_h$ is expressed by the vector $\vec{E}_S$

$$\vec{J}_h = -[\vec{z}_o, \vec{E}_S] \tag{17}$$

Using current formulas for vector components of electrical and magnetic fields of X TE_{10} wave, it's not difficult to deduce a formula for the norm of this wave:

$$N\nu = N_{h10} = \frac{E_m^2}{Z_v} A_h \cdot B_h \tag{18}$$

Where $Z_v = \sqrt{\frac{\mu_a}{\epsilon_a}} / \sqrt{1 - \left(\frac{\lambda}{2A_h}\right)^2}$ is characteristic cross-section impedance of the waveguide

with Ar and Br dimensions for TE_{10} wave; ϵ_a, μ_a are absolute permittivity and absolute permeability of the medium filling the cave of the waveguide; E_m is the amplitude of the TE_{10} wave electrical field in the center of the waveguide cross-section.

After simple manipulations the formula for the TE_{10} wave electrical field is as follows, (there is only one E_y component for the vector $\vec{E}$)

$$E = E_y = \frac{\cos(\pi x / A_h)}{A_h \cdot B_h} \int_{x=-0,5A_h}^{0,5A_h} \int_{y=-0,5B_h}^{0,5B_h} E_{sy}(x,y)\cos(\pi x / A_h) dx \cdot dy \tag{19}$$

where $E_{sy}(x,y)$ is a component of an off-set field (the field of paraboloid) at the horn aperture which is tangent to the horn aperture and parallel to the Y-axis.

The expression for field amplitude E_{max} in the center of the wide side of the horn for power Pr received by horn results from (19):

$$E_{max} = \frac{1}{A_h \cdot B_h} \left| \int_{x=-0,5A_h}^{0,5A_h} \int_{y=-0,5B_h}^{0,5B_h} E_{py}(x,y)\cos(\pi x / A_h) dx \cdot dy \right| \tag{20}$$

$$Pr = E_{max}^2 A_h \cdot B_h / 4Z_v \tag{21}$$

2.4 Double-reflector Cassegrain antenna in radiation mode

In fig.6 a paraboloid (1) and a hyperboloid (2) with additional designations are shown, Oq – the apex of the paraboloid (1); Oq is the apex of the hyperboloid; F1 and F2 are the near and the far foci, N is a point on the hyperboloid surface; R_1 is a distance between F_1 and N points, R_2 is a distance between F_2 and N points. Focus F of the paraboloid and the nearest focus of the hyperboloid coincide. The distant focus of the hyperboloid is agreed with the phase center of the horn. To focus the antenna on the given distance we move the feed-horn – hyperboloid system along the z-axis by Dz distance, to scan – we rotate the hyperboloid around Og point. In figure 6 one of F1-N-M rays is shown as a chain-line.
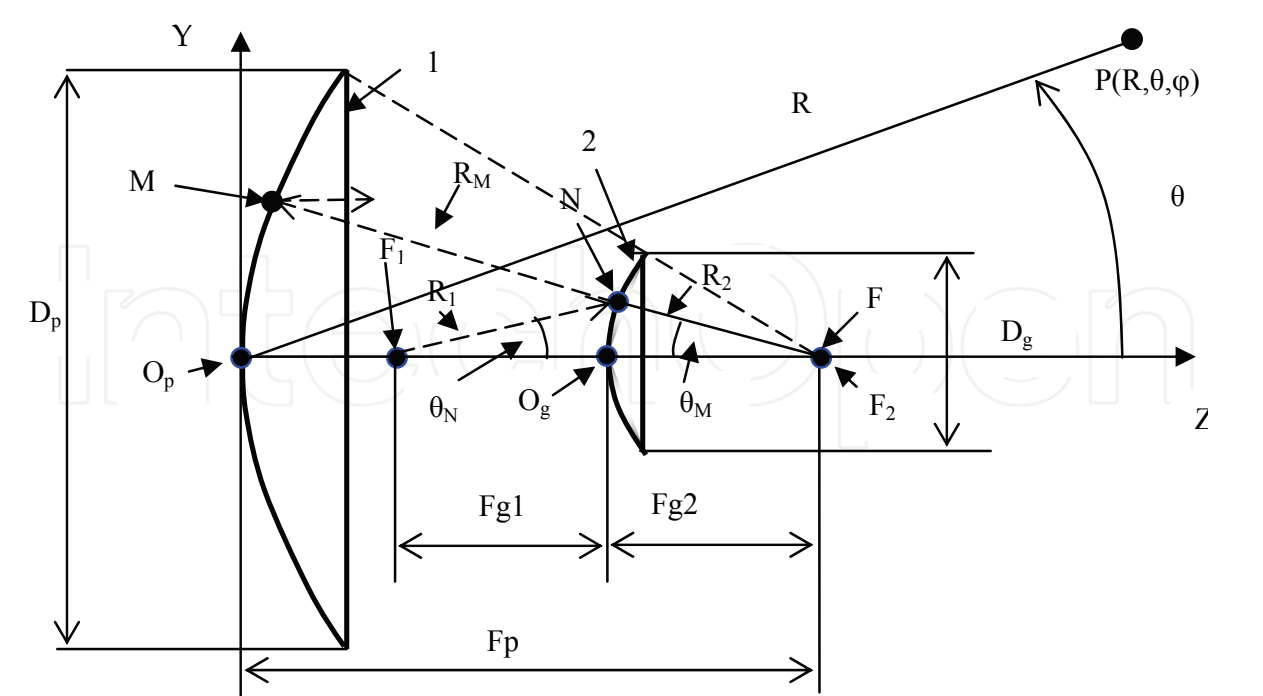
Fig. 6. Paraboloid-hyperboloid system

The configuration of the hyperboloid may be described with the following formulas:

$$R_1 = F_{g2}(1+e)/|1-e\cdot\cos\theta_N| ; \tag{22}$$

$$\mathrm{tg}(0,5\theta_M) = (e+1)/(e-1)\cdot\mathrm{tg}(0,5\cdot\theta_N) \tag{23}$$

where e- is the eccentricity of the hyperboloid (e $\approx$ 1,2…2)

$$e = (F_{g1}/F_{g2}+1)/(F_{g1}/F_{g2}-1) \tag{24}$$

The sequence of antenna field calculation in the point P(R,θ,φ) is the following:
1. Using formula (14) makes it possible to determine the electrical field vector
    $\vec{E}_N(X_N, Y_N, Z_N)$ on the surface of the hyperboloid in the point N and then to calculate
    the vector of the magnetic field strength $\vec{H}_N(X_N, Y_N, Z_N)$. In formula (4) we substitute
    θ_M angle for θ_N angle, R_{QM} for R_{QN}. The angle θ_N is changed in limits

$$0 \le \theta_N \le \theta_{N\max} . \tag{23}$$

The $\theta_{N\max}$ and $\theta_{M\max}$ angles are both performed in formula (23), R_{QN}, is defined by
formula 5 with substituting R_M, θ_M, φ_M coordinates of point M for coordinates of
point N in formula (5):

$$X_N = R_1\cos\theta_N\cos\varphi_N ; \quad Y_N = R_1\cos\theta_N\sin\varphi_N ;$$
$$Z_N = F_p - (F_{g1}+F_{g2}) + R_1\cos\theta_N , \tag{24}$$

where φ_N – an angular coordinate of point N in the XY plane

2. Using the formula which is analogous to formula (9) gives a vector of current density on the hyperboloid surface

$$\vec{J}_{sN} = 2[\vec{n}_o, \vec{H}_N] = \vec{J}_{Nx} + \vec{J}_{Ny} + \vec{J}_{Nz} \qquad (25)$$

3. Knowing $\vec{J}_{sN}$ current we determine the field on the surface of the paraboloid in point M. We use the formula given by (10)

$$\vec{E}_M \approx -i\frac{60\pi}{\lambda}\vec{A}; \quad \vec{A} = \int_{S_g}\vec{J}_{sN}\frac{\exp(-ikR_{NM})}{R_{NM}}dS;$$

$$R_{NM} = \sqrt{(x_N - x_M)^2 + (y_N - y_M)^2 + (z_N - z_M)^2}, \qquad (26)$$

Where S_g is a paraboloid surface.

4. Using the electrical field vector $\vec{E}_M$ we determine the magnetic field vector $\vec{H}_M$ in the point M and then we calculate the current on the surface of the paraboloid and the field in the point P according to formulas (9)-(12). The formulas involved are used in the program for the numerical simulation of different types of reflector antennas as well as for researching field characteristics in the near-field region

3. Results of numerical simulation and its discussion

3.1 The field distribution in the near-field zone in radiation mode

The simulation was made for antennas with the paraboloid diameter $D_p = (10...100)\lambda$ and different ratio F_p / D_p. To demonstrate the main principles we took a single reflector antenna with $Dp = 30\lambda$ and $F_p / D_p = 0.5$ as an example and studied field distribution in the tangent plane (z=const), along the focal axis (z – direction) and depending on the angle θ. The calculations were made for the near-field zone, the intermediate zone and the far-field zone focusing the antenna into the far-field zone and into the given point of the near-field zone. We considered the technology of scanning during focusing the antenna. The sizes of the feed-horn Ah, Bh have been chosen to bring the illumination level of the edge of the reflector with respect to its center in the E and H planes to about 0.3. It coresponds to the maximum antenna gain. All numerical results are given for the plane E.

The distribution of amplitudes and field-phases along the focal axis (Z-distribution) in the near zone is shown in fig.7. The coordinate Z is dependent on the focus point. The antenna is focused on the far-field zone.

It is shown in fig.7 that moving the observation point away from reflector the field amplitude oscillates. Monotonous decrease of the field amplitude begins in the point Z_0. The value of Z_0 and the depth of oscillations increase with the rise of D_p / λ. The reason for the oscillations is the interference of different Fresnel zones at the reflector aperture.

The distribution of the field phase along the focal axis is linear (fig. 7b). It indicates that the traveling field wave propagates along focal axis.

The same situation is observed in the back semi-space, but the oscillations have a less depth and as the distance from the apex of the paraboloid grows the amplitude decreases considerably faster than it happens in the front semi-space.

a) Distribution $|E(Z)| / E\max$ b) Distribution $\arg E(Z)$
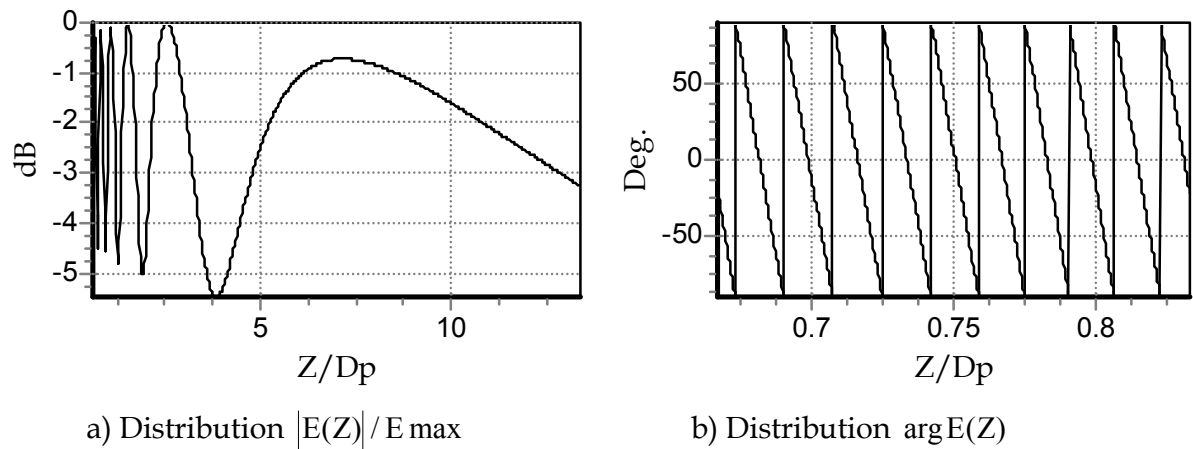
Fig. 7. The field distribution in focal axis direction.

a) R=200 D_P b) R=2,5 D_P c) R=7,5 D_P
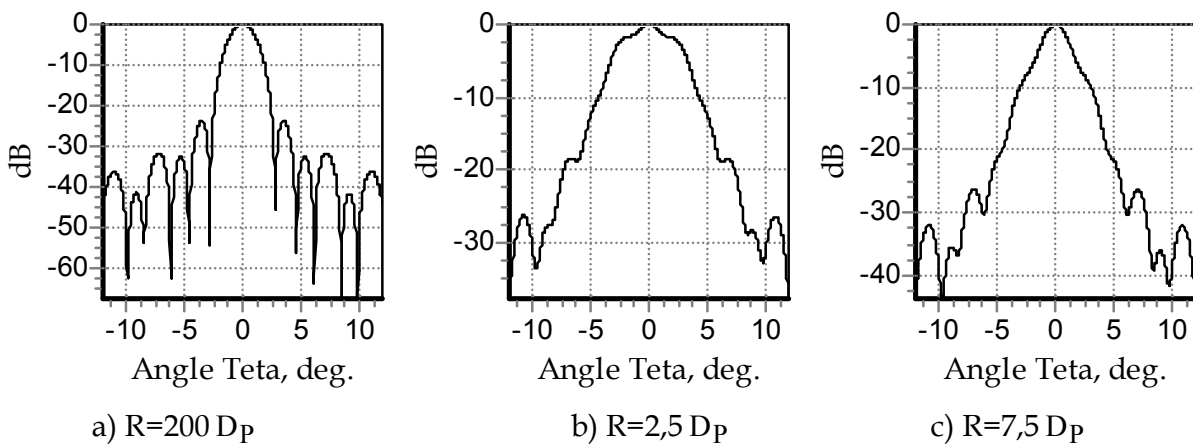
Fig. 8. The antennas field distribution on the sphere R=const.

Neither of amplitude maximum points in figure 7a are an antenna's focusing points. Under a focusing point we mean the point on the sphere, on which the characteristics of distribution of the field amplitude in relation to the angle θ are close to the antenna diagram in the far zone. To illustrate this in fig.8 field distribution on the surface of the sphere R=const for the antenna focused into the far-field zone for distance a) R=200 Dp (antenna diagram); b) R=2.5 Dp; c) R=7.5 Dp (the last two amplitude maximum points are in fig.7)
For comparison in fig.9 it is shown:
the field distribution amplitude on the sphere R=2.5Dp in depending on the angle θ focused on the distance equal to the radius by shifting the feed-horn along the focal axis on $D_{hz} = 1,5\lambda$ (see figure 9 a);
the field amplitude distribution along the focal axis during such shifting of the feed horn (see figure 9 b)
As can be seen from fig.9 b, the field amplitude considerably increases in the focusing point that field distribution depending on the angle θ on the sphere of the antenna, R=2.5Dp focused on this distance is close to the antenna diagram in the far–field zone.

a) Distribution of field on sphere   b) Distribution of field along focal axis
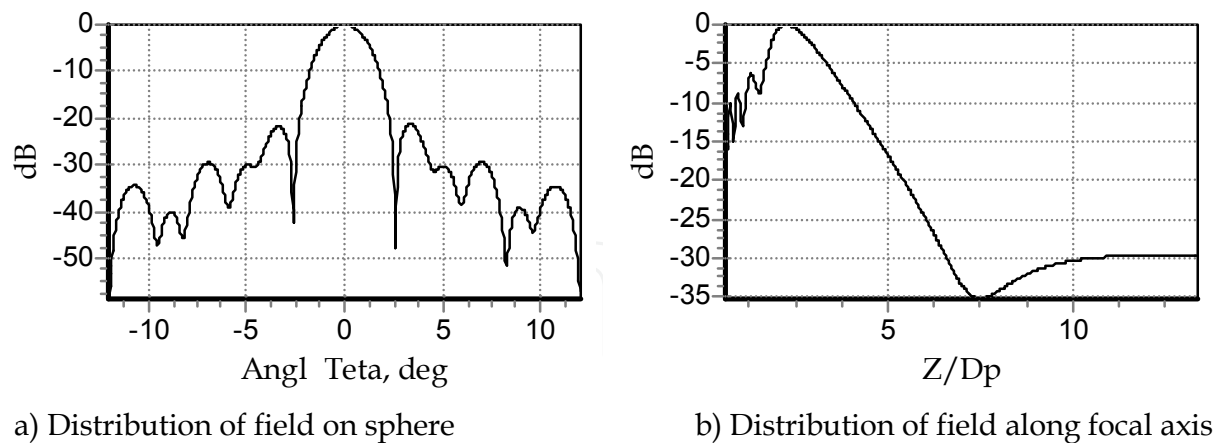
Fig. 9. Field distribution on sphere R=2.5 Dp and along focal axis in antenna focusing case.
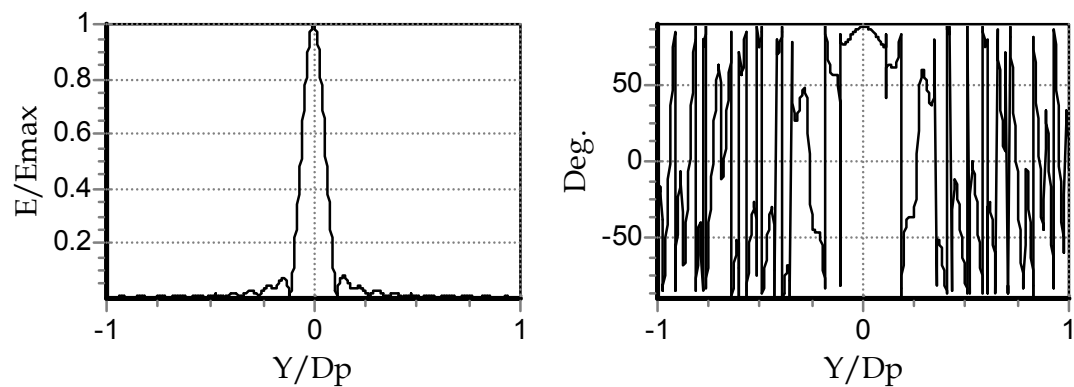
Fig. 10. The amplitude and the field phase in the focusing plane Z=const.

The dependence of the amplitude normalized to the amplitude maximum (E/E_{max}) and the field phase from the coordinate Y in the focusing plane Z=2,5 D_P is shown in fig.10. The value of Y varied within two paraboloid diameter limits ($-D_P \leq Y \leq D_p$).

The region in the y-direction where $E/E_{max} > 1/\sqrt{2}$ will be called the focusing zone and it will be indicated as $\Delta Y_{0,5}$. The value of $\Delta Y_{0,5}$ increases with growing distance to the focusing point and it's linearly related to the diameter of paraboloid. Analogous patterns take place in a double-reflector antenna.

The field distribution in the near-field zone in a spherical wave receiving mode.

The field distribution in the focal region of an antenna during receiving a spherical wave coming from the near-zone is of interest under optimization of the feed-horn position (or several feed-horns in a multi-beam antenna). Further the patterns are demonstrated by the example of an antenna with parameters $D_p = 30\lambda$, F_p / D_p =0,5.

The fig.11 show the field distribution along the focal axis during receiving a spherical wave coming from the point situated a) in the far zone ($R = 200D_p$) b) in the near field zone ($R = 2D_p$). The coordinate Z is counted out from paraboloid apex (point O_P in fig. 6.).

At decreasing distance to the focusing point the width of the region on the focal plane occupied by the main lobe is increasing (fig.11).

It's seen that with fig. 11a the field maximum is located in the paraboloid focus, but with figure 11 b the maximum is moved away paraboloid apex from the reflector on 1.41Fp. If the phase center of the feed-horn is placed in that point, the antenna will be focused on R=2Dp. Fig. 12a depicts the diagram of an antenna focused on the far-field zone at the distance of R=2Dp. It's obvious that differences are discovered only in the side lobe region.

The diagrams of the antenna focused at distance R=200Dp into radiation mode (solid) and receiving mode (Dot) is depicted in fig. 12b. The differences in side lobe region result from different calculation methods, described in the mathematical model.

Fig. 11. The field amplitude distribution along the focal axis.

a) receiving mode:
    solid - $R = 200D_p$;
    dot - $R = 2D_p$

b) Far-field zone:
    dot - receiving mode;
    solid – radiation mode
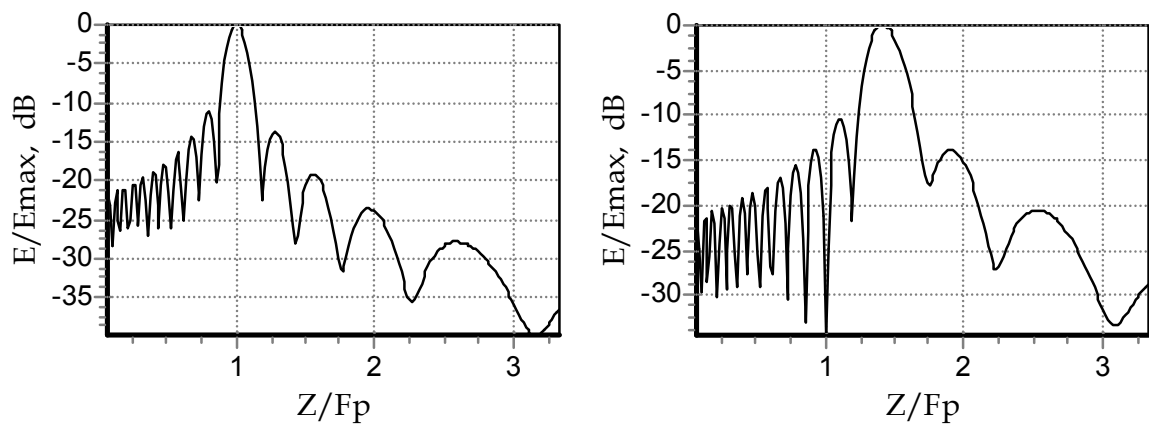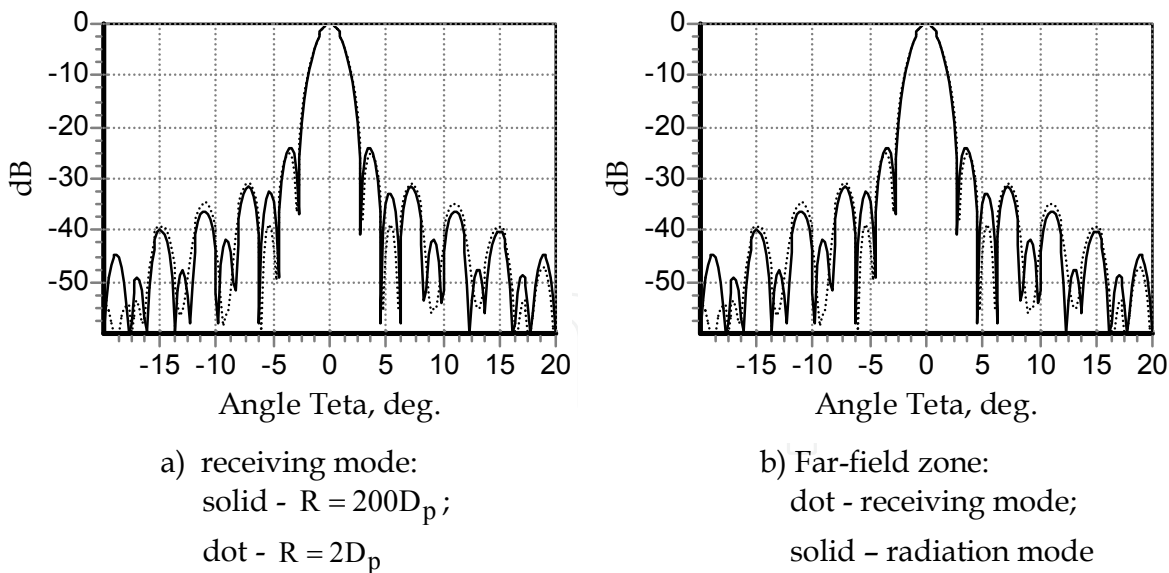
Fig. 12. Antenna diagrams

Scanning in a single-reflector antenna. Multi-beam reflector antenna.

Scanning is produced by moving a feed-horn in a plane Z=const and it is used at the antenna focusing in far-field or near-field zones. Further peculiarities of scanning process at antenna focusing in far-field and near-field zones and features of isolation between channels

in a multi-beam antenna in receiving mode of spherical wave from near-field zone point are considered.

Regularities of scanning are demonstrated by the example of the antenna with the following parameters: D_p =300 mm; F_p =150 mm; f=37 GHz (D_p /λ=37).

The feed horn size Ar, Br are made to be less optimal according to the criteria of antenna gain maximum. This conforms to paraboloid edge illumination level on 10 dB less than in the paraboloid center. The optimal horn sizes for ratio F_p / D_p =0,5 at frequency 37 GHz are the following: A_h =9 mm, B_h =6 mm, R_h =30 mm. The diagrams of the antenna that is focused in the far-field zone at the distance R=200 Dp with three values D_{hy} =0; 20 mm; 40 mm of horn shifting of in the focal plane along Y-axis (see fig.4) are shown in fig. 13. With increasing D_{hy} the main lobe is shifted from the focal axis by the angle Q_m , the beam width $2\theta_{0,5}$ and side lobes level F_{bm} are increased too. These regularities are well-known for far field zones. These regularities remain when the antenna is focused into the near-field zone, but they are quantitatively less expressed. The diagrams with the same parameters D_{hy} for the antenna focused into neat-field zone at the distance R=4 D_p are depicted in fig. 14. The antenna focusing into this distance is produced by shifting the feed-horn along the focal axis at the distance D_{hz} =22 mm (approximately 3λ).
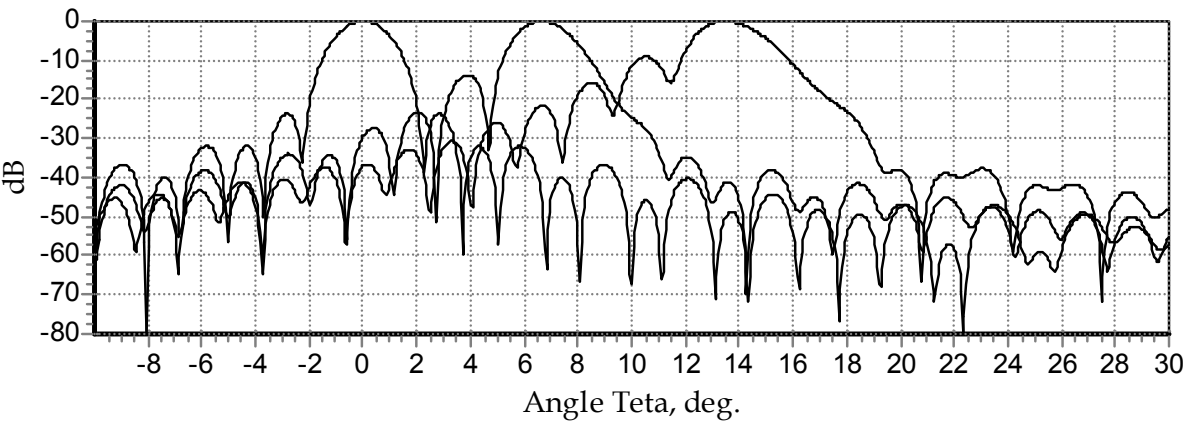
Fig. 13. The antenna diagrams during scanning. The antenna is focused into the far-field zone.
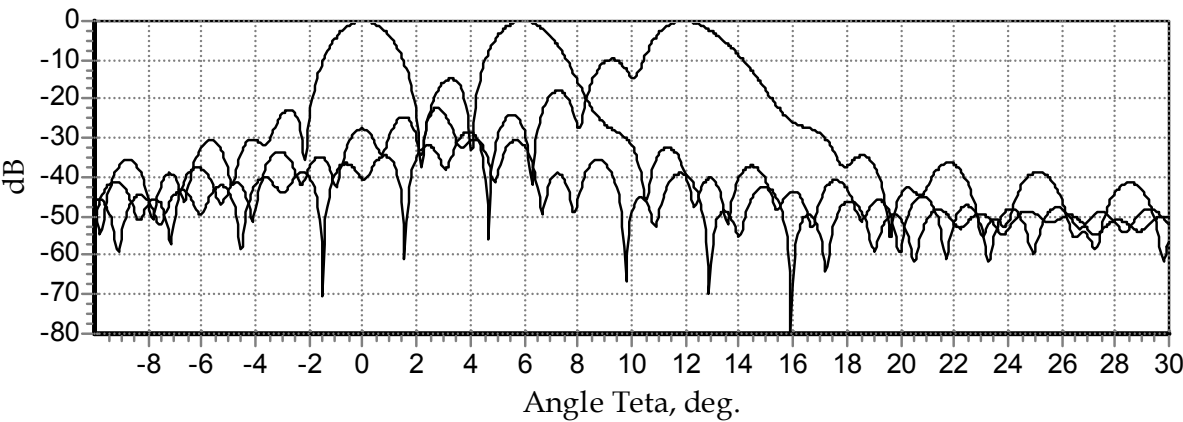
Fig. 14. The antenna diagrams during scanning. The antenna is focused into the near-field zone at the distance R=4 D_P .

The differences of antenna diagrams during scanning and focusing in far-field and near-field zones are illustrated by the following figures.

In fig. 15 the dependence of main lobe deviation angle from the focal axis (Q_m) (15-a) and the dependence of widening the main lobe (DQ%) from shifting the feed horn along Y-axis at focusing into the far-field and near-field zones (15b) shown in fig. 15b. The coefficient of widening the main lobe (DQ %) is determined from equation $DQ\%=[100|2\theta_{0,5}(0)-2\theta_{0,5}|/2\theta_{0,5}(0)$, where $2\theta_{0,5}(0)$ is the width of the not shifted main lobe.

From figure 15 it follows, that the angle deviation of the main lobe from the focal axis and the coefficient of widening are reduced with reducing distance to the antenna focusing point.

The dependence of the coefficient of increasing of side lobe levels (DF) and reducing antenna gain (DG) versus shifting the horn along Y-axis at focusing of antenna in far-field and near-field zones are shown in figure 16. The values DF and DG are given from DF=Fbm-Fbm(0), where Fbm(0) is a side lobe level with the not deviated main lobe; DG=G(0)-G, where G(0) is antenna gain with not deviated main lobe.

a) the deviation angle vs Dny   b) the coefficient of widening vs Dhy
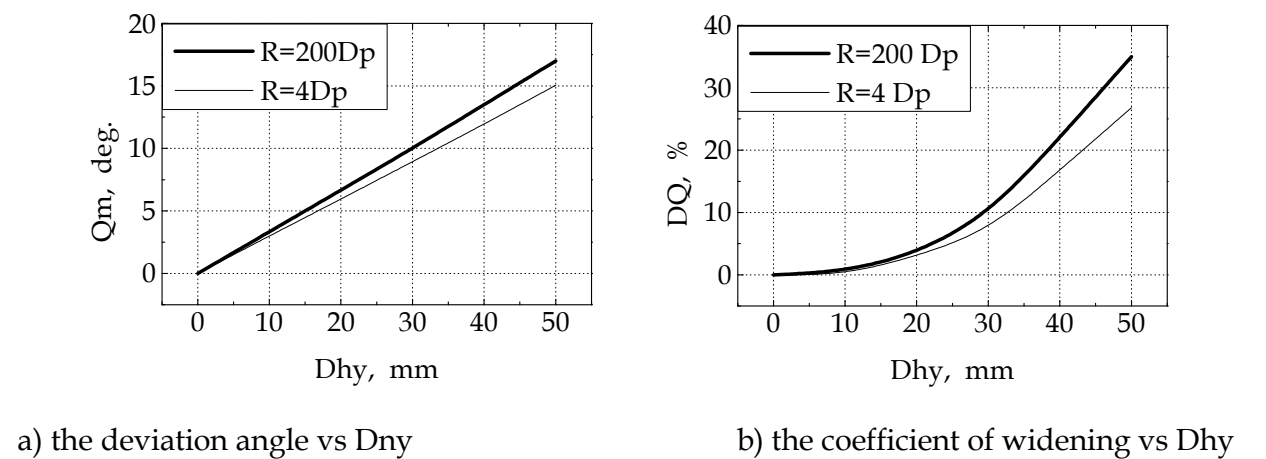
Fig. 15. Scanning in a reflector antenna.

a) An increase of side lobe level at scanning   b) A decrease of gain at scanning
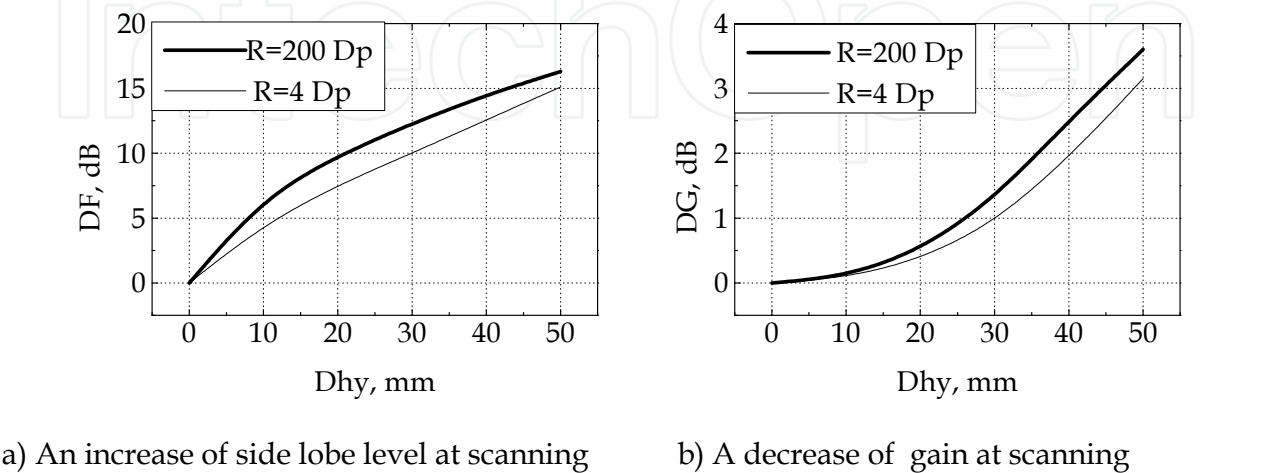
Fig. 16. Changes of antenna parameters at scanning.

From fig. 16 it follows that the effects of increasing the side lobe level and decreasing the antenna gain at scanning are reduced with decreasing the distance to the focusing point.

With increasing D_{hy} the cubic phase error on the paraboloid aperture increases. This results in rapid growth of side lobe levels. Therefore the scanning sector is not great large. It is necessary to decrease a cubic phase error for widening a scanning sector. It is can be made possible by shifting feed-horn along the focal axis additionally by D_{hz0} values. It is demonstrated by the example of the multi-beam antenna with parameters: D_p =300mm; F_p =150mm at frequency 37 GHz. This antenna is focused on the distance $R = 4D_p$ =1200mm. Every beam conforms to one feed-horn in the antenna. The number of feed-horns is $N_h = 30$. The feed-horns are located symmetrically in relation to the focal axis. The coordinates of feed-horns aperture centers along Y-axis are marked as D_{hyn}, on Z-axis – D_{hzn} are. The feed-horns numbers change from -15 up to 15, $-15 \le n \le 15$. The horns with the coordinate D_{hyn} <0 have numbers $-15 \le n < 0$, the feed-horns with coordinates Dhym>0 have numbers $0 < n \le 15$. The feed-horns location along Y-, Z-axis and their size are optimized to the criteria of minimum of side lobe levels and criteria of nearbouring antenna diagram crossing at -3dB level. The antenna diagrams conforming to horns $-1 \le n \le 15$ are shown in figure. 16. The nearest to focal axis horns have numbers $n = \pm 1$.
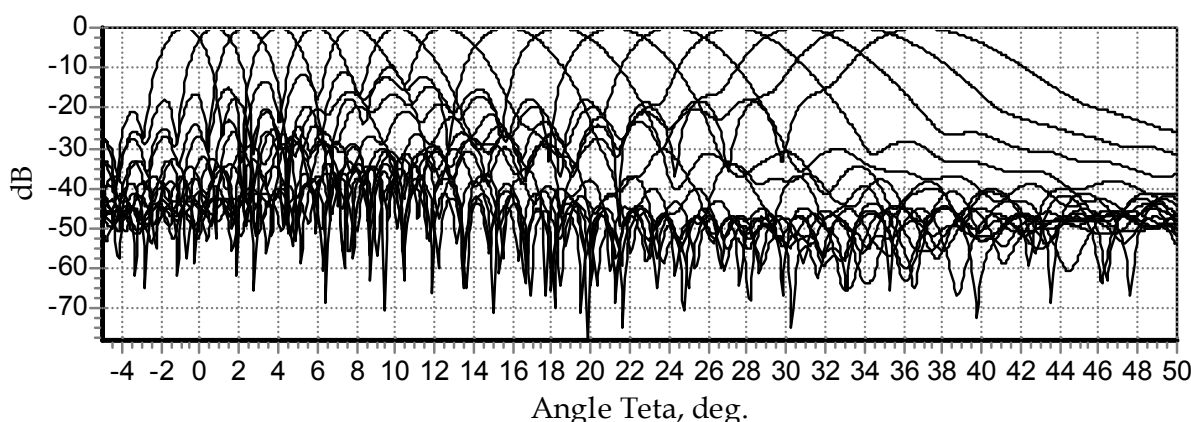
Fig. 17. The antenna diagrams of multi-beam antenna.

From fig. 17 it follows, that by optimization of the feed-horns sizes and location the sector taken up by beams can be essentially widened in comparison with the sector of scanning.

Multi-beam reflector antennas are used in radioimaging systems functioning in the passive mode. In this mode an antenna receives a signals radiated by some object in the near–field or intermediate-field antenna zone. Every reception channel is formed one horn of the feed-horn and receives a signal from the element of allowance on the object. The main lobes of the antenna diagram of the neighboring channels cross at non-zero level (generally it's 0.007 to the maximum). Therefore a signal received from this by the feed-horn of this channel is overlapped by adjacent bin signals (i.e. the desired signal is overlapped by interference and that leads to image degradation). The level of quality degradation can be evaluated as the ratio of the power received from necessary bin on the object to the power received from the adjacent bin in this channel.

Feed-horn isolation depends on the distance between the aperture centers l; on the dimensions of the feed-horn A_h, B_h, R_h; the dimensions of the paraboloid D_p, F_p on;

frequency f. Further the main principles will be considered an with example of an antenna with D_p =300mm, F_p =150mm and f=37GHz. Antenna diagrams of different channels are shown in the fig.17. The example of an amplitude distribution and the field phase distribution in the focus plane Z=const for an antenna focused at the distance of R=4D_p are shown in fig. 17. The spherical wave source point has the following coordinates X=0, Y=0, Z=R. Two feed-horns (depicted as two black triangles) with numbers n=1 and n=5 are also shown. The dimensions of these feed-horns apertures and the coordinates of their centers after optimization of antenna diagrams are the following:

Horn 1- A_h =10,5 mm; B_h =4 mm; D_{hyn} =2,5 mm; D_{hzn} =22 mm

Horn 2 – A_h =10,5 mm; B_h =6 mm; D_{hyn} =27,75 mm; D_{hzn} =26 mm

a) Distribution of amplitude   b) Distribution of phase
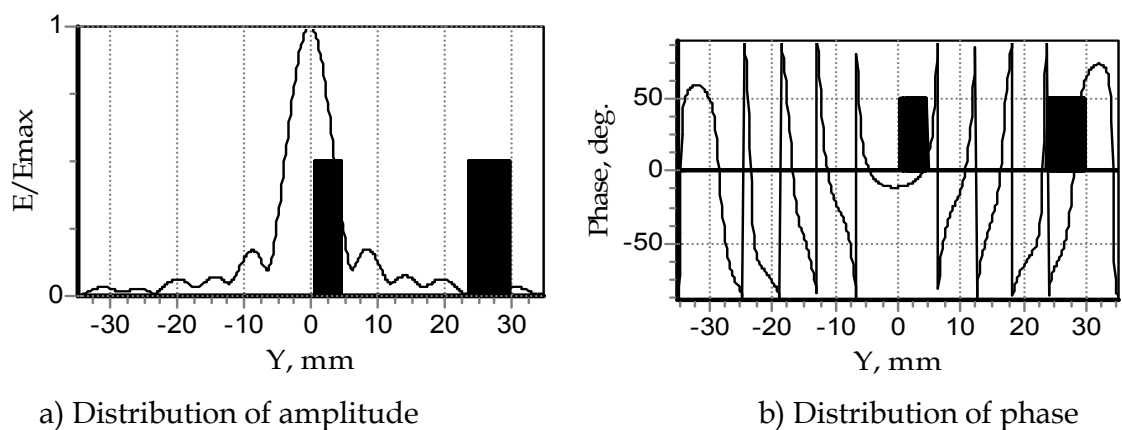
Fig. 18. the distribution of the field amplitude and field phase in the focusing plane Z=const.

From fig.18 it follow that in the focusing plane the amplitude distribution and the field phase distribution are irregular, therefore as the distance between feed-horns increases the excitation amplitude of the feed-horn 2 doesn't decrease monotonous. Therefore the feed-horns isolation in a multi-beam changes monotonous with increasing the distance between feed-horns. The fig.18 depicts the dependence of the isolation coefficient between feed-horn 1 and feed-horns 2, 3,..., 15 depending on the feed-horn number in a multi-beam antenna. The antenna diagram of this antenna is shown in fig.16. The isolation coefficient is given by:

$$P1n = P1/Pn \,, \tag{27}$$

Where P1 is the power received by the feed-horn1; Pn is the power received by the n-th feed-horn. The antenna receives the wave from the point on the Z-axis distant from the apex of the paraboloid at $R = 4D_p = 1200\,$mm.

In fig.19 the similar dependence for an antenna with the feed-horn aperture dimensions and the position in the Y and Z-directions aren't modified according to a criterion of side lobe levels minimum; all the feed-horns have the same dimensions (A_h =10,5 mm; B_h =4 mm) and they are located in the focusing plane Z= D_{hzn} = 22mm. The feed-horns are located along the Y-axis equidistantly. The distance between the centers of the adjacent feed-horns equals 5 mm. At such distance the main lobes of feed-horns 1 and 2 cross each other at the level -3dB. The antenna diagrams conforming to the feed-horns numbered as n=-1…15 are shown in fig. 20.

From fig.16, 19 and 20 it follows that when the antenna receives a spherical wave from a point on the focal plane, the isolation coefficient between the feed-horn in the focusing point (the feed-horn 1) and the adjacent (feed-horn 2) is not less than 16-17 dB. The isolation coefficient at the feed-horn 1 with the rest feed-horns is not less than 20dB. If the feed-horns location in the focusing plane provides crossing the antenna diagrams at the level of -3dB then the level of the side lobes in antenna with the dimensions of the feed-horn corrected in the focusing plane and along the focal axis is distinctly lower than in an antenna without the dimension correction and positions of the feed-horns. The isolation of the feed horns in these two cases doesn't differ much.

a) with dimension correction   b) without dimension correction
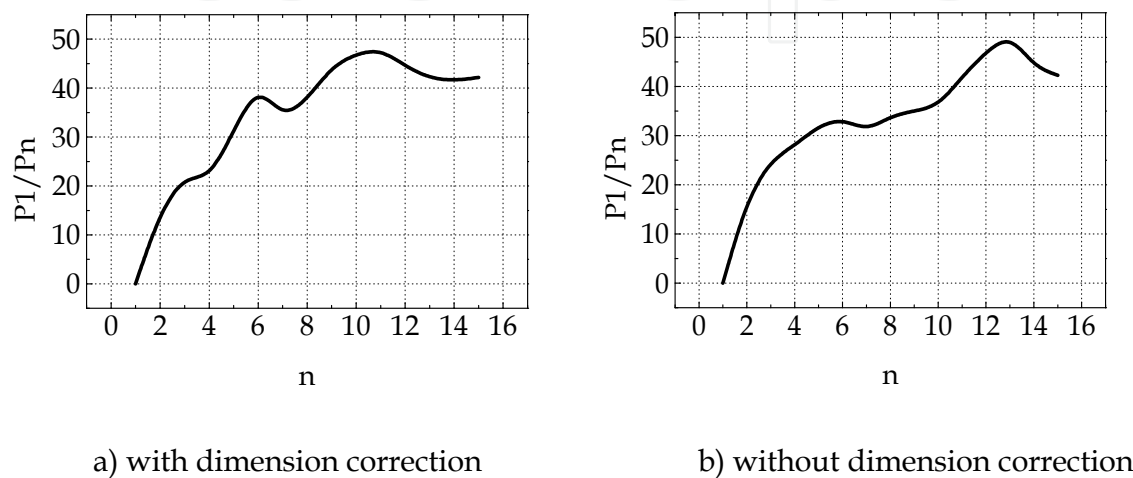
Fig. 19. The dependence of isolation coefficient on feed-horn number.
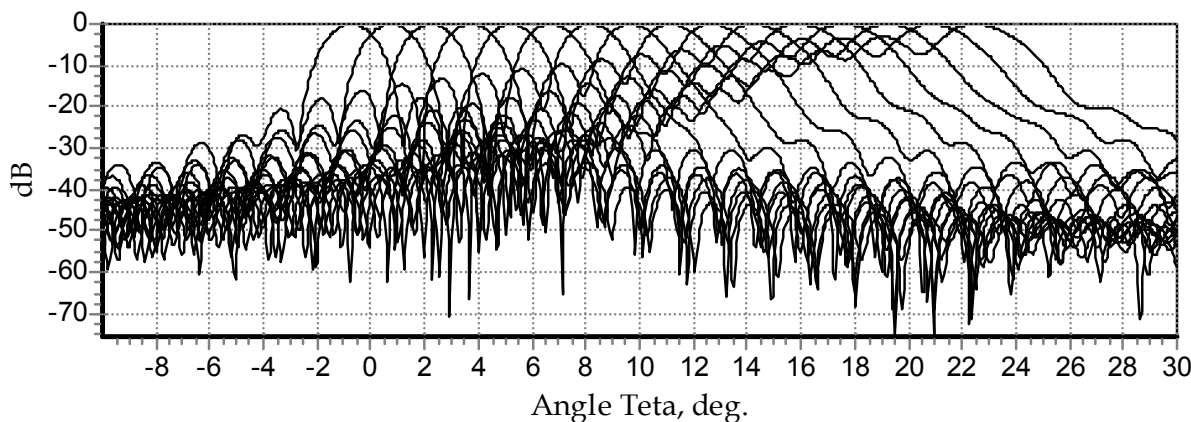
Fig. 19. The antenna diagram of multi-beam antenna without correction of feed-horns dimensions and its location.

When the antenna receives a spherical wave from the point located at $Y \neq 0$ some peculiarities occur. It is connected with the fact that the distribution of field amplitude in the focusing plane is asymmetrical regarding the maximum. Therefore the isolation coefficient between the feed-horn concerned and adjacent feed-horn located to the left and to the right from it is different.

Monopulse double-reflector Cassegrain antenna.

Monopulse antennas are designed for forming two differential diagrams and one sum diagram. The schemes for construction of monopulse double-reflector antennas (MDA) are described in literature. The simplified scheme of a Cassegrain antenna is shown in fig. 22. Designations: 1- is paraboloid (reflector); 2 is a hyperboloid (sub-reflector); 3 – is monopulse horn. The antenna receives a spherical electromagnetic wave coming from the point P (R,0,f) of the far-field zone with angular coordinates 0, f. On the fig. 22 one beam in the receiving mode is depicted in fig. 22 with dotted lines.

The feed-horn must generate three signals: two differential and one summary. Further the numerical modeling results are given and the main principles are described for two types of MDA: a) with a feed-horn in the form of 4-horns executed by TE01 wave mode; b) with a multimode feed-horn. The numerical modeling is produced for antennas with paraboloid diameters the D_p =30λ and the ratio F_p / D_p =0,4. The diameter of the hyperboloid depends on the eccentricity "e" and on the far focal distance Fg1.

A multimode feed-horn is a pyramidal horns with waves TE_{10} , TE_{20} , TE_{11} , TM_{11} . The scheme of simultaneous excitation of these wave modes though the isolated inputs is described in literature. These waves form necessary antenna diagrams: the wave TE_{10} form summary antenna diagram, the wave TE_{20} forms a differential antenna diagram in the magnetic plane (H plane); the sum of waves TE_{11} + TM_{11} forms the differential diagrams in the electrical plane (E plane). The parameters of the antenna diagram of the sum and differential channels depend on the dimensions of the feed-horn cross-section A_h , B_h and the eccentricity E.

Further the dependencies of antenna parameters from A_h , B_h are analyzed. The numerical modeling is produced for antennas with diameters of the paraboloid D_p =30λ and the ratio F_p / D_p =0,4.

The diameter of the hyperboloid depends on the eccentricity E and the distance between paraboloid apex and the feed-horn aperture. The hyperboloid must be inscribed in the aperture angle of paraboloid, as it is shown in fig. 6. The diameter of the hyperboloid D_g must not be larger than 0.25 D_p to reduce the shadow effect. Further results of modeling are given for the case of H=3λ and D_g =0,22 D_P (the eccentricity e=2). For these parameters the level of side lobes in the sum channel in E and H planes is equal and it doesn't exceed -25dB; if the condition A_h =3,33λ; B_h =2,33λ (A_h / B_h =1,428) is fulfilled. The antenna diagrams of the sum channel for the mentioned parameters are shown in fig. 22; in the plane E with a thick line and for H plane with a thin line. The A_h , B_h values, the diameters of hyperboloid D_g and antenna parameters in the summary and differential channels depend on the hyperboloid eccentricity.

The side lobes level and the width of the main lobe of antenna diagram for the summary and differential channels depend on A_h / λ and B_h / λ ratios. With growth of the eccentricity the hyperboloid diameter decreases if the condition of equality of the paraboloid aperture angles and the hyperboloid aperture angle from the focus of paraboloid (the near focus of hyperboloid) is fulfilled. The dependence of the ratio D_g / D_p on the eccentricity E with A_h =3,33λ and B_h =2,33λ is shown in fig. 23. This figure also depicts the dependence of the antenna efficiency factor (Kef) in the summary channel from the hyperboloid eccentricity. The antenna efficiency factor is the value that connects the antenna gain (G), the

area of paraboloid aperture (S) and the wavelength. This relation is determined from well-known formula:

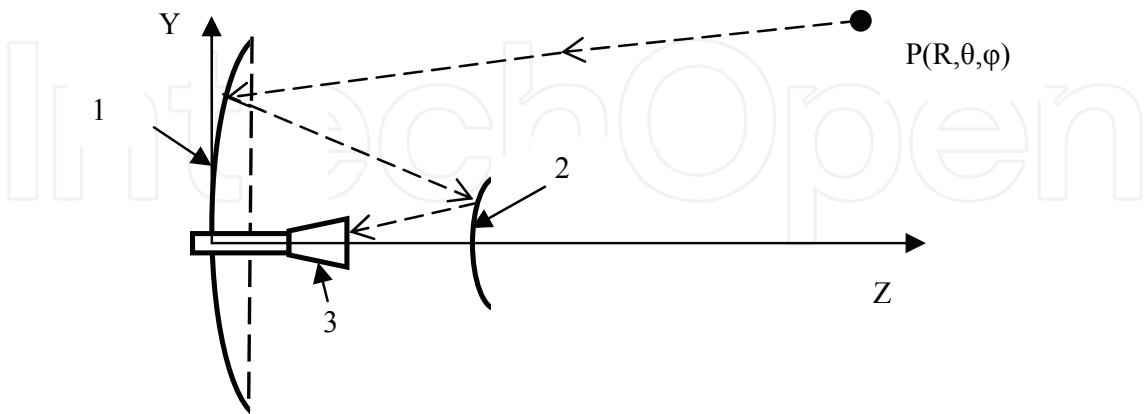$$G = 4\pi \cdot S \cdot Kef / \lambda^2, \text{ the } S = \pi D_p^2 / 4. \tag{28}$$
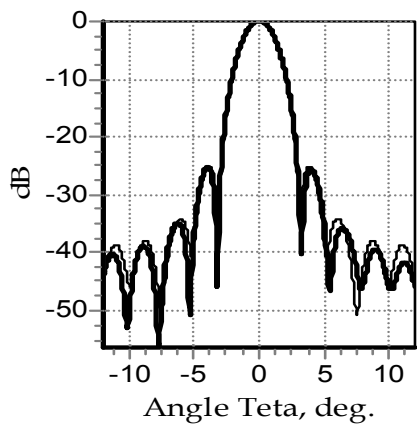

Fig. 22. An Cassegrain antenna scheme.
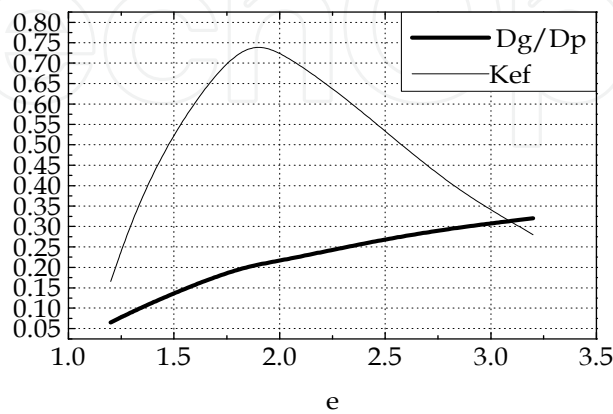

Fig. 23. The antenna diagram for the sum

Fig. 24. The D_g / D_p and Kef versus eccentricity and differential channels.

Depending on the eccentricity the side lobe of summary and differential channels in the E- and H- planes for A_h =3,33λ, B_h =2,33λ change as it is shown in fig. 24. In our calculation we used a lens in the horn to achieve equal phase distribution in the aperture.

With the growth of the eccentricity the hyperboloid diameter increases. Therefore if the values A_h, B_h remain the same the horn field level decreases at the edge of hyperboloid surface. It leads to reducing the side lobes level and to increasing the main lobe width. At the expense of the side lobes reducing the antenna gain increases. At the expense of the main lobe extension the antenna gain decreases.

These two factors lead to the situation when at a certain level of the horn field at the edge of the hyprboloid the antenna gain reaches its maximum. In this case the antenna gain is maximal. Numerical analysis indicates that the maximum of antenna gain in the summary channel is observed when the field level at the edge of the hyperboloid in comparison with the center is $\Delta \approx 0{,}3$.

a) sum channel   b) differential channels
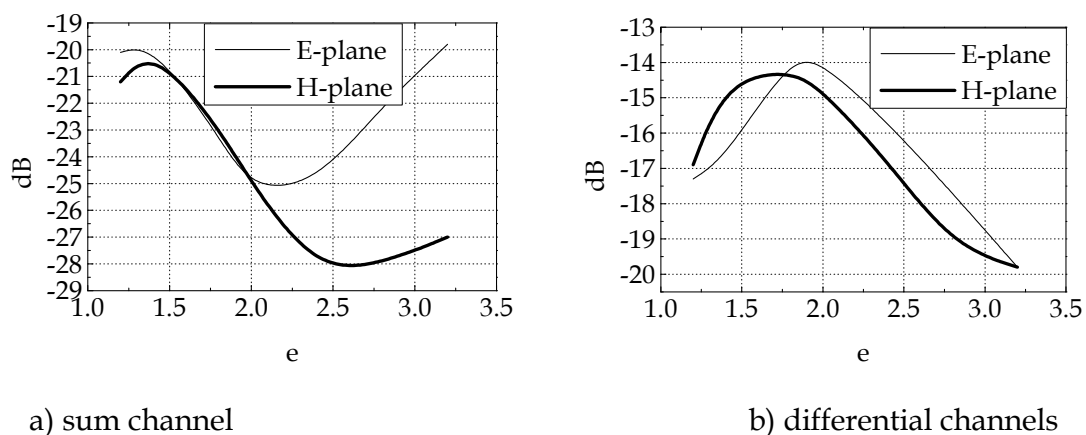
Fig. 24. Side lobe levels versus hyperboloid eccentricity

The dependence of the efficiency factor and the antenna gain in differential channels on the eccentricity is shown on the fig. 24. The maximum of Kef is observed when the level on the edge of the aperture in the plane E is $\Delta_e \approx 0{,}4$; in the plane H is $\Delta_h \approx 0{,}3$.

From fig. 22 it follows that for reducing of side lobes level in the summary channel it's necessary to increase eccentricity in comparison with e=2 besides side lobes in the summary channel in the E- and H-planes are equal. The efficiency factor increases, if E<2.5.

But then the width of main lobe in the summary channel is increased and the antenna efficiency coefficient for the summary channel is decreased.

4. Conclusion

In the chapter the mathematical model of a reflector antenna is described with using the physical optical method and the waveguide excitation theory. New results of research of regularity and parameters of reflector antennas are:

- The field distribution in a near-field zone in a tangent plane and along a focal axis in radiation mode and receiving mode at different wave dimensions of antenna elements; in the receiving mode the antenna is illuminated by a spherical wave from the point with known coordinates, located in any space zone;

- The isolation between channels in a multi-beam antenna in receiving mode of spherical wave, radiated from near-field zone point depending on geometrical parameters of antenna elements.
- Changing diagram parameters of a reflector antenna during scanning and focusing in to given distance.

The results obtained can be used with designing a different purpose antenna.

5. References

Charles, M. An Extension of Rushh's Asymptotic Physical Optics Diffraction Theory of a Paraboloid Antenna. IEEE Trans. Antennas Propagat., vol.23, pp.741-743, Sept., 1975.

Chen, J & Xu, Y. Analysis and Calculation of Radiation Patterns of Cassegrain Antennas. IEEE Trans. Antennas Propagat., vol. 38, pp. 823 – 830.

Fitzgerald, W. The Efficiency of Near-Field Cassegrainian Antennas. IEEE Trans. Antennas Propagat., AP-14, no.9, pp.648-650, Sept. 1972.

Hannan, P.W. *Optimum feeds for all three modes of a monopulse antenna I: Theory*, IRE Trans. Antennas Propagat., vol. 9, pp. 444 - 454, September 1961.

Houshmand, D; Lee, S-W; Rahmat-Samii, Y & Lam, P. Analysis of Near-Field Cassegrain Refletctor: Plane Wave Versus Element-by-Element Approach. 1988 IEEE Int. Antennas Propagat. Symp. Dig. vol. 26, pp. 124 - 127, June 1988.

Khayatian, B; Rahmat-Samii, Y; *Characteristics of dual reflector antennas with gaps placed on the subreflector: MoM and PO analysis*, 1999 IEEE Int. Antennas Propagat. Symp. Dig. vol. 37, pp. 2332 - 2335, June 1999.

Laybros, S; Combes, P.F.; &Mametsa, H.J. The «Very-Near-Field» Region of Equiphase Radiating Apertures. IEEE Antennas & Propagation Magazine. 2005, vol. 47, No.4, pp.50-66.

Narasimhan,M; Ramanujam,P; & Raghavan, K. *GTD analysis of a hyperboloidal subreflector with conical flange attachment*, IEEE Trans. Antennas Propagat., vol. 29, pp. 865 - 871, November 1981.

Narasimhan, N and Christopher S. A New Method of Analysis of the Near and Far Fields of Paraboloidal Reflectors. IEEE Trans. Antennas Propagat., AP-32, no.1, pp.13-19, January 1984.

Narasimhan M & Govind, K. Front-to-back ratio of paraboloidal reflectors, IEEE Trans. Antennas Propagat., vol. 39, pp. 877 - 882, July 1991.

Rahmat-Samii, Y. *Subreflector extension for improved efficiencies in Cassegrain antennas-- GTD/PO analysis*, IEEE Trans. Antennas Propagat., vol. 34, pp. 1266 - 1269, October 1986.

Rahmat-Samii, Y; *Jacobi-Bessel analysis of reflector antennas with elliptical apertures*, IEEE Trans. Antennas Propagat., vol. 35, pp. 1070 - 1074, September 1987.

Radar Handbook. Editor-In-Chif Skolnik M.I. McGraw_Hill Book Company, 1970.

Rusch, W. Physical-optics diffraction coefficients for a paraboloid. Electronic Lett., vol.10, pp.358-360, Aug.22, 1974.

Valentino, A & Toulios,P. Fields in the Focal Ragion of Offset Parabolic Antennas. IEEE Trans. Antennas Propagat., vol. 24, pp. 859 - 865, November 1976.

Watson, W. The Field Distribution in Focal Plane of a Paraboloidal Reflector. IEEE Trans. Antennas Propagat., vol. 12, pp. 561 - 569, September 1964.

Numerical Simulations - Applications, Examples and Theory

Edited by Prof. Lutz Angermann

ISBN 978-953-307-440-5

Hard cover, 520 pages

Publisher InTech

Published online 30, January, 2011

Published in print edition January, 2011

This book will interest researchers, scientists, engineers and graduate students in many disciplines, who make use of mathematical modeling and computer simulation. Although it represents only a small sample of the research activity on numerical simulations, the book will certainly serve as a valuable tool for researchers interested in getting involved in this multidisciplinary ï¬eld. It will be useful to encourage further experimental and theoretical researches in the above mentioned areas of numerical simulation.

How to reference

In order to correctly reference this scholarly work, feel free to copy and paste the following:

Oleg Yurtcev and Yuri Bobkov (2011). Numerical Modeling of Reflector Antennas, Numerical Simulations - Applications, Examples and Theory, Prof. Lutz Angermann (Ed.), ISBN: 978-953-307-440-5, InTech, Available from: http://www.intechopen.com/books/numerical-simulations-applications-examples-and-theory/numerical-modeling-of-reflector-antennas

INTECH
open science | open minds